Asian Journal of Civil Engineering
https://doi.org/10.1007/s42107-022-00516-x

ORIGINAL PAPER

Generating seismic fragility curves of RC frame building using NSPA and IDA

Kaushik Gondaliya[1] · Jignesh Amin[2] · Vishisht Bhaiya[1] · Sandip Vasanwala[1] · Atul Desai[1]

Received: 15 February 2022 / Accepted: 3 October 2022

Abstract

In the last two decades, seismic fragility analysis for RC frame buildings has become critical in evaluating structure risk and safety margin due to lateral loads. In the study, the four-storey RC frame building is designed per the latest IS 1893 for seismic zone-V. Multiple fragility analysis methodologies are compared using nonlinear static pushover analysis and incremental dynamic analysis (IDA). The fragility curve for the capacity-spectrum method (CSM) was calculated using spectral displacement (S_d) as per ATC-40 instructions, and an uncertainty factor was calculated using the approximate methodology of normal (continuous) to the binomial (discrete) distribution. Traditional IDA, multiple stripe analysis, and truncated IDA curve-fitting approach produce fragility curves from IDA results. Traditional IDA results are more accurate than the others based on the coefficient of variation when examining the fragility curves for selected RC frame buildings in Surat City.

Keywords Uncertainty estimation · Incremental dynamic analysis (IDA) · RC frame · Fragility analysis · Capacity spectrum-based method (CSM)

Abbreviations

ADRS	Acceleration–displacement response spectra
COV	Coefficient of variation
CSM	Capacity-spectrum method
DL	Dead load
EDP	Engineering demand parameters
GM	Ground motion
IDA	Incremental dynamic analysis
LL	Live load
MIDR	Maximum inter-storey drift ratio
MSA	Multiple stripe analysis
NSPA	Nonlinear static pushover analysis
RTR	Record to record
SD	Standard deviation
SSE	Sum of squared errors

List of symbols

d_b	Diameter of longitudinal reinforcement in metre
f_y	Yield stress of longitudinal reinforcement in MPa
$GM_{1,i}$	*i*Th record of the first horizontal component
IM_i	IM value associated with the onset of collapse for the *i*th ground motion
L	Length of the member in metres (taken at the point of contra flexure from the end)
n	Number of ground motions
$NGM_{1,i}$	Normalised *i*th record of the first horizontal component
NGM_i	Normalisation factor of both horizontal components of the *i*th record
Pk	Probability of occurrence
S_d	Spectral displacement
$S_{d,ds}$	Mean spectral displacement
z	Collapses occurring for a total number of ground motions
β	The standard deviation of a natural logarithm

✉ Kaushik Gondaliya
d19am007@amd.svnit.ac.in; kgondaliya51@gmail.com

Jignesh Amin
prof_jignesh@gtu.edu.in

Vishisht Bhaiya
Vishisht@amd.svnit.ac.in

Sandip Vasanwala
SAV@amd.svnit.ac.in

Atul Desai
AKD@amd.svnit.ac.in

[1] Department of Civil Engineering, Sardar Vallabhbhai National Institute of Technology, Surat, Gujarat, India

[2] Graduate School of Engineering and Technology, Gujarat Technological University, Chandkheda, Gujarat, India

Published online: 18 October 2022

Θ Mean value of the normal distribution
Φ The standard normal cumulative distribution function

Introduction

Structural designers and researchers have been trying to reduce dynamic loading like earthquakes and wind, causing massive destruction. The exponential growth of India's population and the construction of large cities like Surat City, characterised by insufficient land occupation, contribute to increased damage caused by seismic disasters. These zones have a high concentration of people, buildings, infrastructure, and exposed values, making them seismically at very high risk. The strong Bhuj earthquake-2001 struck in the twentieth century, killing almost 20,000 people. The majority of casualties were caused by the collapse of structures. New constructions and, to a lesser extent, restoring older ones benefitted from advances in structural design. However, there are far more old buildings than modern ones.

High-rise and tall structures use the passive, active, semi-passive or hybrid damper system to overcome seismic risk and provide an economical building design (2021b; Bhandari et al., 2019; Sharma et al., 2021a). In a developing country like India, most of the structure's height is low-rise (up to 8 m) and mid-rise (up to 15 m). Indian building owners cannot afford the structural member's expensive structural system and heavy reinforcement detailing. Fragility analysis can be essential in government seismic risk management policies and mitigation strategies.

Fragility analysis is the study of obtaining the fragility curve to give the probability of failure due to seismic conditions. To accurately predict the structural reaction, two factors in the fragility function are critical, namely the mean (μ) and standard deviation (β), which describe the fragility function's demand threshold limit and uncertainty, respectively (Porter, 2014). Many Indian researchers have derived the fragility analysis for Indian building structures to estimate post-seismic structure response (Choudhury & Kaushik, 2018; Surana et al., 2015). Researchers have observed that engineers failed to assess the uncertainty correctly concerning the Indian circumstances. In the case of seismic fragility, uncertainty rises from three main factors: variability in mathematical modelling, demand spectrum (earthquake ground motion/response spectrum), and threshold of damage states (Hazus-MH MR5, 2001). The seismic performance limit of the structure considered for damage measure is known as engineering demand parameters (EDP). Structure response took EDP as the peak storey displacement/drift, maximum inter-storey drift ratio (MIDR), and spectral acceleration. They collected the EDP data using various mathematical and analytical techniques. The fragility curves can be derived using nonlinear static pushover analysis (NSPA) and incremental dynamic analysis (IDA) for RC frame buildings. Tables 1 and 2 show the brief latest literature summary of deriving the fragility curve using NSPA and IDA.

The likelihood of reaching or exceeding a particular damage state as a function of a parameter defining the seismic action to which the building is subjected to a specific damage state is described by a fragility curve. Table 3 shows the various fragility functions used, particularly in the RC frame buildings, for the derivation of the fragility curves. In Eq. (1) lognormal probability density function is commonly assumed to describe fragility curves accurately.

$$P[\mathrm{DS} \geq \mathrm{DS}_k | X = \Theta] = \Phi\left[\frac{1}{\beta_\mathrm{k}} \ln\left(\frac{\Theta}{\mu_\mathrm{k}}\right)\right]. \quad (1)$$

This study's process is a detailed seismic fragility assessment methodology for a single structure under a particular ground motion (GM) or elastic design spectrum. The inter-storey drift ratio was chosen as the critical damage-generating metric, since it is substantially connected with earthquake damage. The following paragraphs go over the stages involved in this technique.

1. The presented methodology necessitates the NSPA or IDA nonlinear analysis of an idealised computer model of the provided structure. Information about the building must be gathered, such as as-built geometry, features, and material properties obtained from in situ tests.
2. The computer creates a two-dimensional model based on the structure and the analyst's preference. Similarly, the analyst selects the nonlinear analysis type, such as NSPA or IDA. If a nonlinear static analysis is performed, one of the methodologies available in the literature (e.g., ATC, 1996; HAZUS®-MH MR5, 2003; Barbat et al., 2006) is used to estimate the building's performance point, the prescribed GM or elastic design spectrum. The deformations of the RC frame at the performance point are recorded. The maximal member end deformations are directly recorded when a nonlinear IDA is performed.
3. The established fragility function is used to derive fragility curves using each curve-fitting method utilising the obtained maximum member end deformations from Step 2.
4. After determining the damage measure for each approach, the curve-fitting function for each method is computed to identify the best fit for the four-storey RC frame building. The residual error is affected by the curve-fitting function's contribution, the analytical method utilised, and the collected deformation distribution type. This article develops approximate values for these parameters.

Table 1 Summary of the RC frame structures' fragility analysis: Part-I

S no.	Research information					Special modelling features
	References	Building type	Building height (m)	Software used	Local/regional	
1	Adom-Asamoah and Osei (2018)	RC frame	9	OpenSees	Local	A single rotational spring model
2	Choudhury and Kaushik (2018)	RC frame with Infill wall	14	SAP2000	Local	Nonlinear behaviour of the infill masonry wall in RC frame
3	Moon et al., (2018)	RC frame	10.74	ZEUS-NL	Local	Structural irregularity in plan
4	Serdar Kirçil and Polat (2006)	RC frame	20.30	IDARC-2D	Local	3-, 5- and 7-storey RC frame 220 and 420 reinforcement grades
5	Ji et al., (2007)	RC frame	184	ZEUS–NL	Local	Development of a lumped-parameter model for sample building
6	Mitropoulou et al., (2016)	RC frame	25	SCADA Pro	Local	A fixed model where soil–structure interaction is neglected, a spring model with single-node Winkler springs, pile foundation model where soil–structure interaction is simulated using beam and quadrilateral
7	Nazari and Saatcioglu (2017)	RC frame with shear wall	20	PERFORM 3D	Local	Shear wall modelling in RC frame building
8	Dabaghi et al., (2019)	RC frame with shear wall	36	OpenSees	Local	The effect of varying the number of storeys, shear wall, and boundary conditions Element dimensions and reinforcement detailing the seismic collapse fragility
9	Su et al., (2020)	RC frame with Infill wall	18	OpenSees	Local	Unreinforced masonry in the RC frame building model
10	Surana et al., (2018)	RC frame	27.50	ETABS	Regional	Buildings are classified with foundation arrangement,
11	Pejovic and Jankovic (2016)	RC frame with a core wall	120	PERFORM 3D	Local	20-, 30- and 40-storey RC high-rise buildings
12	Kiani and Pezeshk (2017)	RC frame	Not specified	OpenSees	Local	3-, 6-, 9- and 12-storey RC moment-resisting frame
13	Zaker Esteghamati et al., (2018)	RC frame with core walls	105	OpenSees	Local	20-, 25- and 30-storey RC moment-resisting frame
14	Bhandari et al., (2019)	RC frame	32	SAP2000	Local	10-storey RC frame building isolated by lead rubber bearing (LRBs)
15	Bilgin (2016)	RC	14	SAP2000	Local	Three types of RC health care facilities in Turkey
16	Arabzadeh and Galal (2017)	RC frame with core walls	45	OpenSees	Local	12-storey RC frame building designed and retrofitted
17	Kyriakides and Pantazopoulou (2018)	RC frame	–	–	Local	–

Table 1 (continued)

S no.	Research information					Special modelling features
	References	Building type	Building height (m)	Software used	Local/regional	
18	Tavazo and Ranjbaran (2017)	RC frame	Not specified	OpenSees	Local	The endurance time (ET) method explained

Table 2 Summary of the RC frame structures' fragility analysis: Part-II

S no.	Analysis type						Post-processing		
	Static/ dynamic	Type of GMs	Number of GMs used	Type of fragility analysis	IM	EDM	Total number of analyses	Fragility model	Function fitting method
1	Dynamic	Synthetic	180 (Artificial)	Cloud based	S_a	MIDR	180	Gaussian	LLS
2	Static	–	–	MM	S_a	S_d	23	LN	Not specified
3	Dynamic	Unscaled	15 (Recorded)	MCS	PGA	MIDR	23,000	LN	LLS, MM
4	Dynamic	Unscaled	12 (artificial)	IDA with linear regression	PGA, S_d, S_a	MIDR	12	LN	LLS
5	Both	Not specified	30 (recorded)	Not specified	S_a	Drift	600	LN	Not specified
6	Static	–	–	Not specified	S_a	Displacement	–	LN	Not specified
7	Dynamic	Scaled	20 (recorded)	IDA	S_a	Drift	Not specified	N	Not specified
8	Dynamic	Not specified	22 (recorded)	Truncated IDA	S_a	MIDR	Not specified	LN	MLE, MM
9	Dynamic	Unscaled	20 (recorded)	LHS, MCS	PGA	MIDR	1520	LN	MM
10	Dynamic	Not specified	Not specified	IDA	S_a	MIDR	Not specified	LN	Not specified
11	Dynamic	Scaled	60 (recorded)	IDA	PGA	MIDR	3600	N	LLS
12	Dynamic	Unscaled	745	Cloud based	S_a	MIDR	1490	LN	MLE, LLS
13	Dynamic	Unscaled	22	IDA	S_a	MIDR	Not specified	LN	LLS
14	Dynamic	Scaled	40	IDA	S_a	MIDR	Not specified	LN	LLS
15	Dynamic	Unscaled	100	Time history	PGA	Drift	–	LN	LLS
16	Dynamic	Scaled	50	IDA	S_a	MIDR	750	LN	MLE
17	Static	–	–	–	PGA	Drift	–	LN	Not specified
18	Dynamic	Scaled	100	IDA, ET	S_a	MIRD	1500	LN	MLE

5. The procedure's final step is to compute the coefficient of variance based on the computed curve-fitting approach to compare the accuracy.

Characteristic of GMs

A significant amount of GM data is necessary to cover a variety of possible building responses. For reliable estimations of median capacity, 17–20 GMs should be enough, as per FEMA P695 (2009). GM intensity variation is frequently illustrated using a site-specific hazard curve, which ties spectral intensity to exceedance frequency. Most hazard curves, on the other hand, are regional. Studying the literature on Surat City, the researcher derived hazard curves, and all basic parameters were selected from these studies to represent the current local condition (Mohanty & Verma, 2013; Shukla & Choudhury, 2012;

Table 3 Fragility curve-fitting function used in the past literature for deriving fragility curves

Authors	Fragility function	Parameters
Baker (2015) and Vamvatsikos and Allin Cornell (2002)	$P\,[\text{Collapse}\vert\text{IM}=x]=\Phi\left[\frac{1}{\beta}\ln\left(\frac{x}{\Theta}\right)\right]$	Where IM is the intensity measure of ground motions; S_d; θ is the mean spectral displacement where a building ranges the damage grade threshold; β is the standard deviation of a natural logarithm of spectral displacement for damage grades
Barbat et al. (2008) and Kappos et al. (2006)	$P[\text{ds}\geq\text{ds}_k\vert X=S_d]=\Phi\left[\frac{1}{\beta_k}\ln\left(\frac{S_d}{S_{d,ds}}\right)\right]$	S_d is the spectral displacement, $S_{d,ds}$ is the mean spectral displacement where a building ranges the damage grade threshold; β_k is the standard deviation of a natural logarithm of spectral displacement for damage grades
Jeon et al. (2012)	$P\,[D\geq C\vert\text{IM, IDS}]=\Phi\left[\frac{1}{\sqrt{\beta_{d\vert\text{IM}}+\beta_c+\beta_m}}\ln\left(\frac{S_d}{S_{d,ds}}\right)\right]$	Where IM is the intensity measure of ground motions; S_d and $\beta_d\vert$IM are the median value and dispersion, respectively, of the demand as a function of IM; $S_{d,ds}$ and β_c are the median value and distribution, respectively, of the capacity; β_m is the modelling uncertainty;
Saruddin and Nazri (2015)	$P\,[\text{Damage}\vert\text{IM}=\text{PGA}]=\Phi\left[\frac{1}{\sigma}(\ln(\text{PGA})-\mu)\right]$	Where D is damage, μ is the mean, and σ is the standard deviation of the natural logarithm of PGA
McCrum et al. (2016)	$P\,[\text{ds}\vert S_d]=\Phi\left[\frac{1}{\beta_{ds}}\ln\left(\frac{S_d}{S_{d,ds}}\right)\right]$	Where $S_{d,ds}$ is the median value of spectral displacement at which the building reaches the threshold of the damage state, ds; β_{ds} is the standard deviation of the natural logarithm of spectral displacement of damage state, ds
Pejovic and Jankovic (2016)	$P\,[\text{DS}_i=\text{IDR}>\text{IDR}^{\text{DS}i}\vert\text{IM}]=\Phi\left[\frac{1}{\sigma}(\ln(\text{IM})-\mu)\right]$	The basic parameters of the fragility curve are the mean value μ and standard deviation σ

Φ is standard normal cumulative distribution

Thaker et al., 2012). Various scalable intensity measure (IM) parameters should be considered while conducting an incremental dynamic analysis (IDA). The typical IM parameters are the peak ground acceleration (PGA), peak ground velocities (PGV), and the 5% damped spectral acceleration at the first-mode period ($S_a(T_1,5\%)$). Numerous studies demonstrated that spectral acceleration ($S_a(T_1,5\%)$) was recognised as a good choice for IM (Luco & Cornell, 2007; Verki & Aval, 2020).

Due to the insufficient number of recorded earthquakes in the developing countries under consideration, it is common practice to adopt records from other regions that may not belong to the same seismic plateau, but are comparable in terms of earthquake magnitude and source-to-site distance, and local geological and subsoil conditions. A small number of ground movements with similar seismic properties have been employed in this study. It is essential to select a wide range of GMs to perform IDA. Current GM selection strictly uses the properties representing the Surat City soil properties and intensity of past earthquakes (Sairam et al., 2019). Table 4 summarises the incident's size, year, and the station's name for each record. The far-field record set contains 32 records ranging from 6.5 to 7.62, with an average magnitude of 7.07. For the far-field record set, the shortest site–source distance is 18.82 km, the maximum length is 98.22 km, and the average distance is 45.56 km, based on the average epicentral distances.

Numerical example

The NSPA and IDA techniques investigated the fragility of a four-storey RC building frame. NSPA and IDA are conducted to generate lateral load and far-field site-specific seismic demand measurements, respectively, and then compared to a group of defined damage states. The following subsections cover the modelling and designing of the RC frame, normalisation and scaling of the selected GMs, and performance criteria for choosing damage states examined in the study.

Mathematical modelling and design

Four-storey typical special moment-resisting RC frame buildings were used as research objects, and the considered structure frame model geometry and rebar detailing are shown in Fig. 1. RC frame has a bay width of 4 m, and the ground and upper storey are 3.5 m in height. The total weight of the infill walls is considered at all levels to reflect a widely used study and design technique that ignores the strength and stiffness of masonry infill walls. The centre frames of the buildings are chosen to derive fragility curves. Gravity loads are classed as either dead (IS 875: Part-1 1987) or live (IS 875: Part-2 1987) according to IS 875 (1987). The self-weight of beams, columns, slabs, and walls is considered a dead load. The slab, internal, and external walls have 125 mm, 115 mm, and 230 mm thickness, respectively. Live loads of 3 kN/m^2 and 0.75 kN/m^2 are used for

Table 4 Summary of earthquake events and recording station data from PEER dataset

ID	RSN	Event/station	Magnitude	Vs_{30}	Epicentral distance
1	20	Northern Calif-03/Ferndale City Hall	6.50/M_w	219.31	30.79
2	68	San Fernando/LA—Hollywood Stor FF	6.61/M_w	316.46	39.49
3	730	Spitak, Armenia/Gukasian	6.77/M_w	343.53	36.19
4	754	Loma Prieta/Coyote Lake Dam (Downst)	6.93/M_w	295.01	30.89
5	848	Landers/Coolwater	7.28/M_w	352.98	82.12
6	850	Landers/Desert Hot Springs	7.28/M_w	359.00	27.32
7	1100	Kobe, Japan/Abeno	6.90/M_w	256.00	46.73
8	1101	Kobe, Japan/Amagasaki	6.90/M_w	256.00	38.79
9	1158	Kocaeli, Turkey/Duzce	7.51/M_w	281.86	98.22
10	1186	Chi-Chi, Taiwan/CHY014	7.62/M_w	347.63	66.19
11	1602	Duzce, Turkey/Bolu	7.14/M_w	293.57	41.27
12	1628	St Elias, Alaska/Icy Bay	7.54/M_w	306.37	74.83
13	3749	Cape Mendocino/Fortuna Fire Station	7.01/M_w	355.18	30.04
14	4849	Chuetsu-oki/Kubikiku Hyakken Joetsu City	6.80/M_w	342.74	46.72
15	5823	El Mayor-Cucapah/Chihuahua	7.20/M_w	242.05	20.63
16	5827	El Mayor-Cucapah/Michoacan de ocampo	7.20/M_w	242.05	18.82

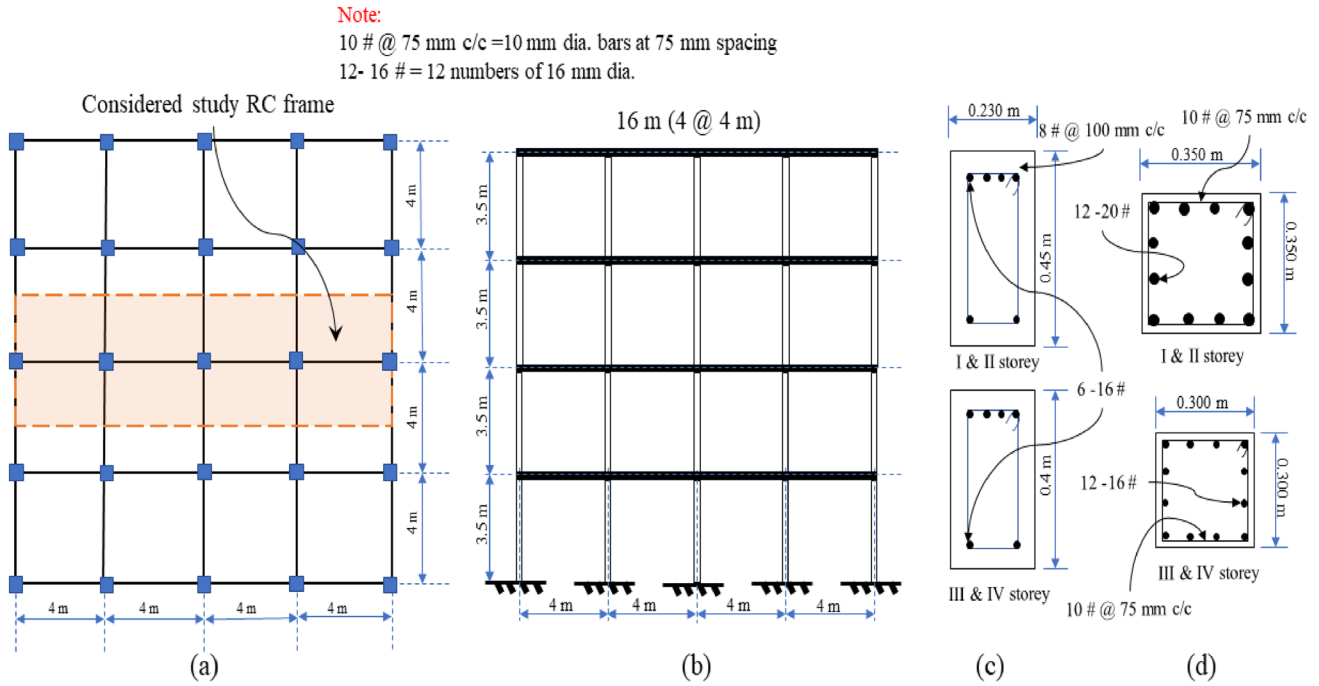

Fig. 1 Structural geometry and rebar detailing of selected RC frame building: **a** plan, **b** elevation, **c** column and **d** beam

stories and roofs, respectively. The materials utilised in this investigation are standard weight concrete with a compressive strength of 25 MPa, steel reinforcements with a yield strength of 500 MPa, and a modulus of elasticity of 200 GPa. IS 456 (2000), IS 1893 (2016), and IS 13920 (2016) are used into the design of 4-storey RC frame building.

Nonlinear frame elements with concentrated plasticity simulated the beam and column elements. The stress–strain curve of concrete is described using Mander's model (Mander et al., 1988). The stress–strain envelope in each concrete fibre in a section is calculated using the Mander model. The reinforcing bars are characterised using the hysteresis model based on kinematic hardening behaviour often found in metals (Prota et al., 2009). The Takeda hysteresis model defines its properties, or the strength and stiffness deterioration for each loading and unloading (Menegotto & Pinto, 1973). The

final curvatures are utilised to calculate the rotation values using the full plastic hinge length. The plastic hinge length proposed by Priestley et al. (1996) is adopted in this work as per equation (2):

$$L_p = 0.08\,L + 0.022\,f_y d_b, \tag{2}$$

Plastic hinges (only flexural) are assumed to form at a distance of $l_p/2$ from the face of beams and columns. Figure 2 represents the flow of the current study to derive the fragility curve using various analytical and statistical approaches.

Normalisation and scaling of selected GMs

According to FEMA P695 (2009), the GM record sets contain a sufficient number of records to analyse record-to-record (RTR) variability. GM data is scaled to represent a specific intensity level. First, the data in each set are "normalised" by their peak ground velocities. This stage removes unjustifiable variability among forms due to inherent differences in event size, distance to the source, source type, and site conditions without removing the overall RTR variability. Equations (3, 4) were used to normalise the selected GM from the PEER-NGA database.

$$\mathrm{NGM}_i = \frac{\mathrm{Median}\left(PGV_i\right)}{PGV_i}, \tag{3}$$

$$\mathrm{NGM}_{1,i} = \mathrm{NGM}_i \times \mathrm{GM}_{1,i} \text{ and } \mathrm{NGM}_{2,i} = \mathrm{NGM}_i \times \mathrm{GM}_{2,i}. \tag{4}$$

Next, all normalised GMs are scaled to a certain target response intensity so that the GM set's median spectral acceleration matches the fundamental time period (T_a). Table 5 summarises key record information from the downloaded GM from the PEER-NGA database for each GM. The record sequence number and the file names of the two horizontal components are included in this information. The maximum values of as-recorded peak ground acceleration (PGA), PGA_{max}, and maximum values of as-recorded peak ground velocity (PGV), PGV_{max}, are also included in each record. The term "maximum" implies that the larger value of the two horizontal components is presented. PGA_{max} is 0.30 g on average, with PGA ranging from 0.10 to 0.81 g. With PGV values ranging from 20.55 to 65.88 cm/s, the average PGV_{max} is 37.06 cm/s. The normalisation factors range from 0.54 to 2.01. Following normalisation, PGA values vary from 0.16 to 0.52 g, with an average PGA_{max} of 0.31 g. Table 6 shows that normalisation of the records (by PGV from PEER) has reduced the dispersion in PGV_{max} to a level consistent with that of PGA_{max} without appreciably affecting average values of PGA_{max} or PGV_{max} for the record set. Figures 3 and 4 show the scaling of the GM and mean scaled GM with the maximum target response spectra zone-V.

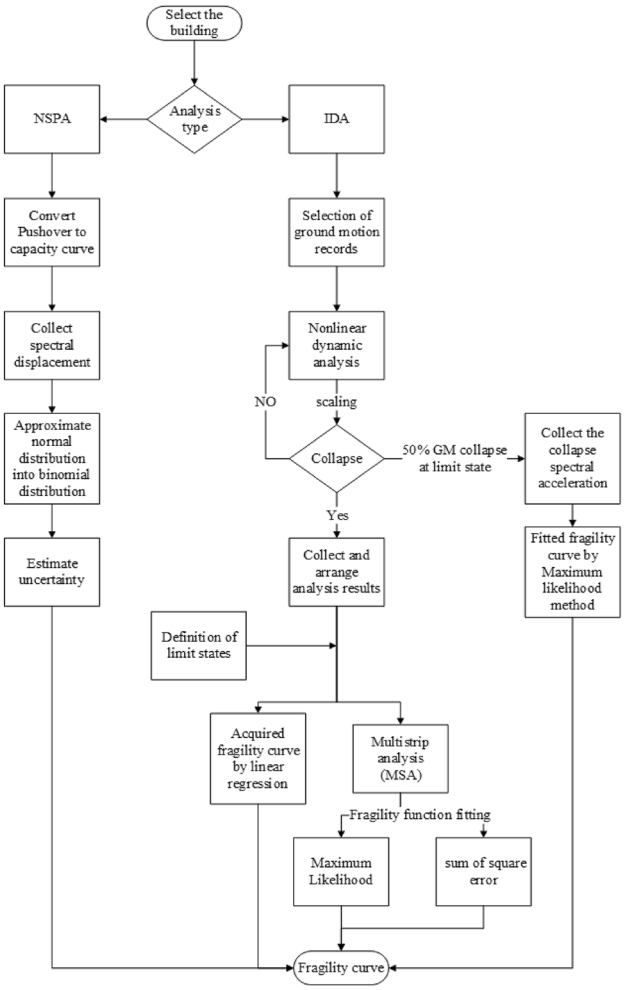

Fig. 2 Flowchart of adopted methodology in the present study

Performance limit state criteria

Fragility curves are derived using the pre-defined threshold limit suggested by international standards (FEMA P695, 2009; Hazus-MH MR5, 2001). As shown in Eq. (5), it has established a damage grade threshold derived from the building structure's yielding and ultimate spectral displacement:

$$S_{\mathrm{d,k}} = \begin{cases} 0.7D_y & \text{Slight} \\ D_y & \text{Moderate} \\ D_y + 0.25\left(D_u - D_y\right) & \text{Severe} \\ D_u & \text{Complete} \end{cases}, \tag{5}$$

where D_y is the yield spectral displacement and D_u is the ultimate spectral displacement of the capacity curve, and it is crucial to define the performance limit criteria for the structure's response. The literature observed that the maximum

Table 5 Factors are calculated and used to normalise typical GM parameters following FEMA P695

ID	PGA		PGV		PGV_{max}	PGA_{max}	Normalise factor	Normalise PGV_{max}	Normalise PGA_{max}
	H_1	H_2	H_1	H_2					
1	0.16	0.20	36.07	26.21	36.07	0.20	1.06	38.35	0.21
2	0.22	0.19	21.72	16.94	21.72	0.22	1.70	37.01	0.37
3	0.20	0.17	28.36	14.98	28.36	0.20	1.59	44.98	0.32
4	0.16	0.18	13.42	22.72	22.72	0.18	1.87	42.53	0.34
5	0.28	0.42	27.62	43.42	43.42	0.42	0.94	40.99	0.40
6	0.17	0.15	19.46	20.88	20.88	0.17	1.62	33.86	0.28
7	0.22	0.23	21.25	24.78	24.78	0.23	1.42	35.30	0.33
8	0.28	0.33	33.57	44.83	44.83	0.33	0.84	37.78	0.28
9	0.31	0.36	58.87	55.66	58.87	0.36	0.57	33.62	0.21
10	0.26	0.10	23.05	11.43	23.05	0.26	2.01	46.42	0.52
11	0.74	0.81	55.93	65.88	65.88	0.81	0.54	35.48	0.44
12	0.10	0.10	19.97	20.55	20.55	0.10	1.61	33.16	0.16
13	0.33	0.28	33.91	38.05	38.05	0.33	0.91	34.63	0.30
14	0.21	0.25	38.63	43.89	43.89	0.25	0.79	34.84	0.20
15	0.25	0.20	38.34	33.99	38.34	0.25	0.91	34.72	0.23
16	0.54	0.41	61.55	43.54	61.55	0.54	0.63	38.87	0.34

Table 6 Comparison of the maximum, minimum, and average values of peak ground acceleration (PGA_{max}) and peak ground velocity (PGV_{max}) for recorded and normalised GM

Parameter value	PGA		PGV	
	Recorded	Normalised	Recorded	Normalised
Max	0.81	0.52	65.88	46.42
Min	0.10	0.16	20.55	33.16
Ratio max/min	8.10	3.24	3.20	1.39
Average	0.30	0.31	37.06	37.66

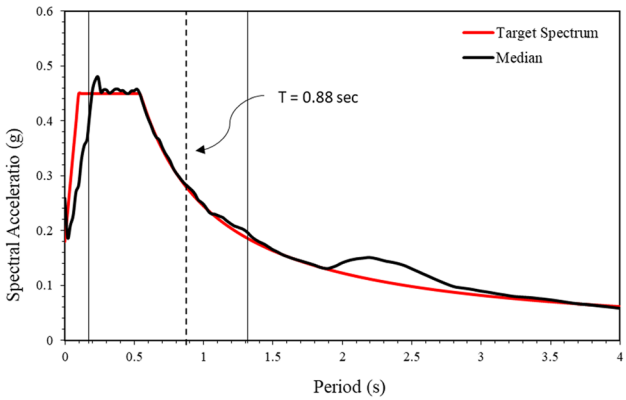

Fig. 3 Mean spectral response with target response spectrum for seismic zone-V as per ASCE

inter-storey drift ratio (MIDR) provides precise output for predicting the structure's behaviour (Banerjee et al., 2016; Bhandari et al., 2019). The results are shown in boxplots in

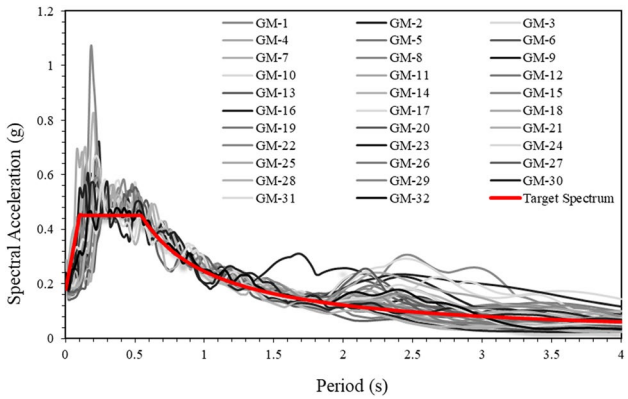

Fig. 4 Response spectra of 32 GMs are scaled for the target seismic zone-V spectrum

Fig. 5, where the solid line illustrates the range of variation from the lower to upper bond for each intensity measure. The box shows the interquartile range (Q_3–Q_1), which begins at the lowest and ends at the highest. The median is reached by drawing a vertical solid line inside the box quartile. The time history analysis' inter-story drift ratio for various IM values to specific storey height is shown in Fig. 6.

Nonlinear static pushover analysis (NSPA)

Nonlinear static pushover analyses are generally known as pushover analyses. NSPA is conducted under the factored gravity load combination equal to DL + 0.25*LL and static lateral forces. Pushover analysis is conducted per section 3.3.3 of ASCE/SEI 41 (2017) guidelines. The vertical

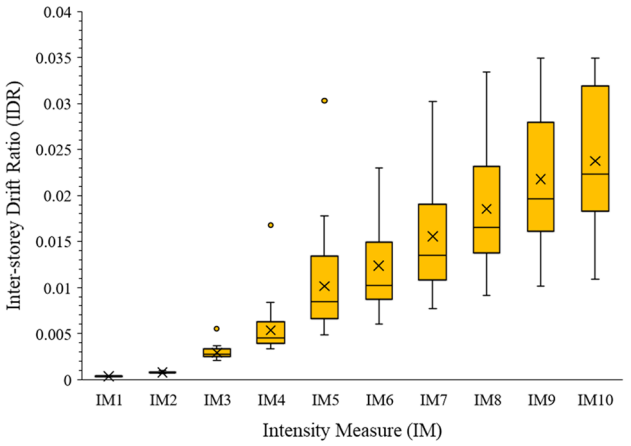

Fig. 5 Inter-storey drifts ratio of 4-storey buildings for each selected scaled IM value

distribution of the lateral load, F_x, at each storey level, x, should be in proportion to the fundamental mode shape of the RC frame building model using Eq. (6) according to IS:1893-2016 (Part-I):

$$Q_i = \frac{W_i h_i^2}{\sum_{i=1}^{n} W_i h_i^2} V_{\mathrm{d}}. \tag{6}$$

The seismic design force is denoted as Q_i at the ith floor, the seismic weight is indicated as W_i at the ith floor, and the floor ith measured from the base is expressed as h_i. Ahead of the incremental seismic forces, the vertical building loads are allocated. Figure 7a shows the pushover analysis results that give the base shear vs displacement. Further, these values are converted into the spectral acceleration (S_{a}) vs spectral displacement (S_{d}) (see Fig. 7b), typically known as the capacity curve. Conversion of the capacity curve as per ATC-40 has been done using the powerful toolkit package provided by SAP2000 software (CSI software, 2006).

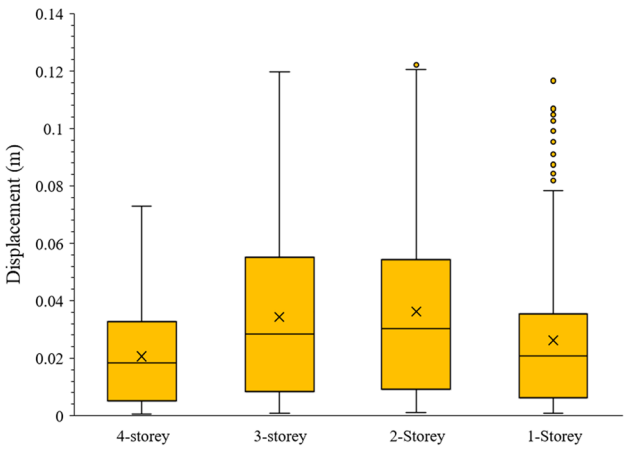

Fig. 6 Displacement collected for scaled IM levels at each storey level of the selected building

Incremental dynamic analysis (IDA)

Time history data are scaled to each GM in a suit until the structure collapse is referred to as IDA (Vamvatsikos & Allin Cornell, 2002). Instead of employing incremental lateral loads on the structure, like in NSPA, the real-time history of previous earthquakes is applied. As a result, it is a more reliable and widely acknowledged approach in the twenty-first century. The 32 GMs are scaled to different intensity levels determined by PGA and applied to the selected RC frame structure. Values ranging from 0.05 to 2 with 0.2 uniform increments were used to cover the PGA range. Increments can be either scaled or unscaled. Observations made indicate that scale increments performed better for estimating DM, whereas unscaled increments are more commonly used to analyse tall structures (Vamvatsikos & Allin Cornell, 2002). 320 nonlinear time history studies for X-direction seismic activities are performed for the specified ground movements. On a machine with an 11th Gen Intel® Core (TM) i5-1135G7 @ 2.40 GHz

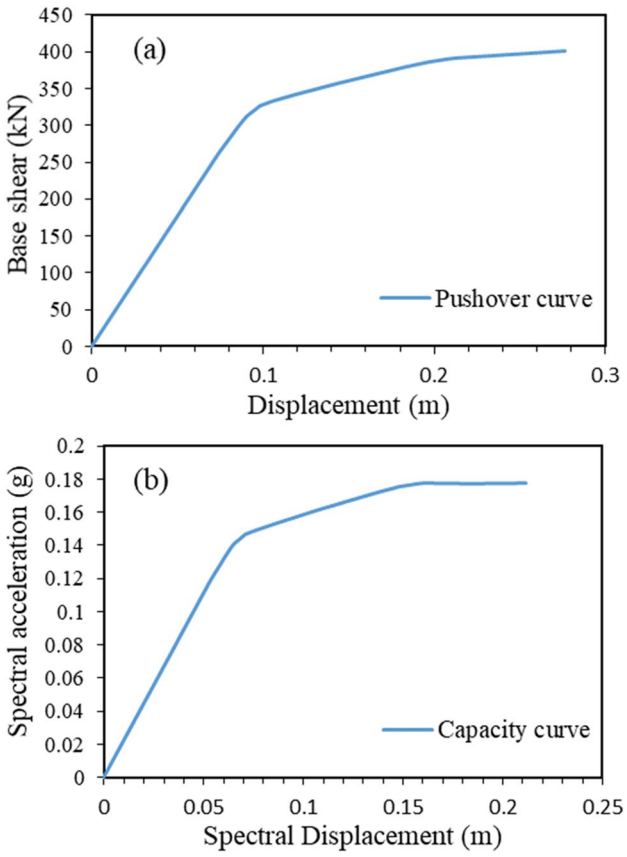

Fig. 7 **a** Pushover curve converted into the **b** capacity curve as per the ATC-40

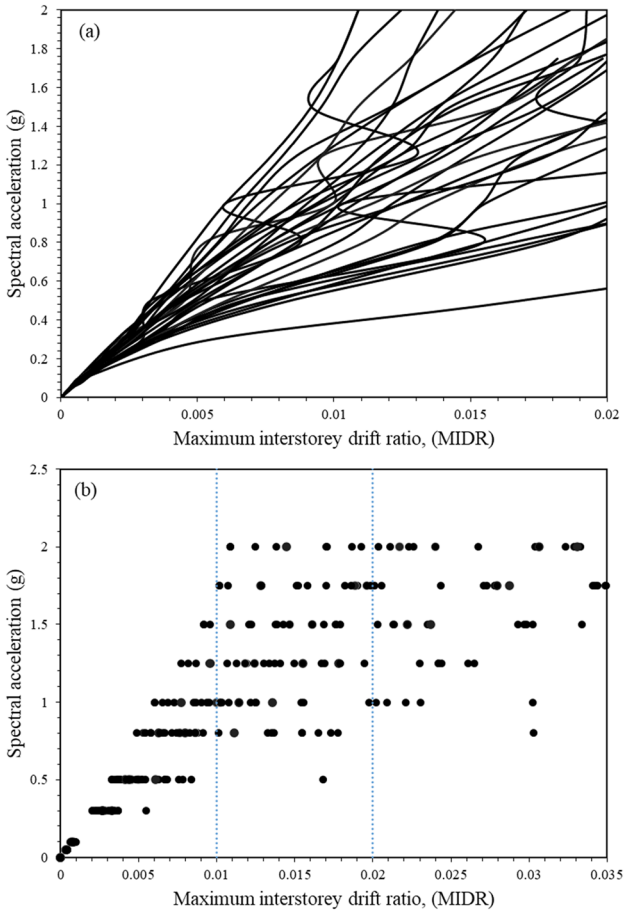

Fig. 8 IDA result for identifying spectral acceleration (Sa) associated with MIDR for each ground motion represented in **a** and **b**

and 1.38 GHz and 8 GB of RAM, this took about 370 h to complete. The Python programming language utilised the fragility curves for each damage condition. The resulting MIDR values at each damage state's threshold was determined by ASCE 41 (2017). Figure 8 shows the collected IDA results of the four-storey RC frame building.

Fragility curve-fitting techniques

Capacity-spectrum method (CSM)

Naive Lantada et al. (2009) and Alex Barbat et al. (2008) calculate the expected total uncertainty in structure and seismic demand using the CSM. The pushover curve is converted into the capacity curve (ADRS format) as per the ATC-40 recommendation to find the performance point for a particular seismic demand. The spectral displacement (S_d) is assumed to follow a binomial probability distribution, as defined in Eq. (7), to estimate the value of β_k:

$$P_k = P(\mathrm{DS} = \mathrm{DS}_k) = P_k(N,d) = \sum_{k=0}^{n-1} \binom{n-1}{k} d^k (1-d)^{n-1-k}; \quad k = 0, \ldots, (N-1). \tag{7}$$

The damage grades are denoted as N, taken as 5 in this study. The value of $d = \mathrm{DS}_m/N - 1$ represents the damage level, ranging from 0 to 1. The value of $d = 0$ indicates no damage to a structure. However, the value of $d = 1$ indicates complete damage in a frame. Further, Eq. (1) is fitted to the obtained point through Eq. (7) through the least square criterion. Table 7 represents the particular damage grades fixed at 50%, in which parameter d controls an assumed binomial probability distribution. Figure 7 shows an example of fragility curves obtained through this method. It shows the probability of expecting damage grade while fixing a 50% probability for a sample four-storey RC frame building. Further, the likelihood of exceedance (P_k) is determined through the seismic hazard specification of a designed RC frame building. It is done through fragility curves by selecting the probability of exceedance at a corresponding performance-point spectral displacement (S_d) (Table 7).

Thus, the probability of occurrence (p_k) for each damage state is obtained from the corresponding fragility curves by subtracting the accepted succeeding damage state exceedance probability, as per the following Eq. (8):

$$p_k = P_k(k+1) - P_k(k). \tag{8}$$

Table 7 Probabilities of the expected damage grade after fixing 50% probability for each damage state, mean, uncertainty and CoV

Damage states	Fixing condition	d	DS_1	DS_2	DS_3	DS_4	$S_{d,ds}$	β	CoV
Slight	$Sd_1 = 0.5$	0.19	0.500	0.192	0.049	0.009	3.83	0.35	0.09
Moderate	$Sd_2 = 0.5$	0.39	0.845	0.500	0.178	0.038	4.17	0.41	0.10
Severe	$Sd_3 = 0.5$	0.63	0.989	0.862	0.500	0.149	4.62	0.48	0.10
Complete	$Sd_4 = 0.5$	0.85	1.000	0.996	0.905	0.500	4.78	0.61	0.12

$S_{d,ds}$ is denoted as the logarithmic value of the spectral displacement for calculating the coefficient of variation (CoV)

It is to be noted that this probability of exceedance value is derived for the optimum beta (β_k) value use of equation (9) to estimate a fragility function by minimising the sum of squared errors (SSE) between normal and binomial distribution (Fig. 9):

$$\hat{\beta} = \underset{\beta}{\arg\min} \sum_{j=1}^{m} \left[\mathrm{P} - \sum_{k=0}^{N} kP_{\mathrm{k}}(N,d) \right]^2. \tag{9}$$

Multiple strip analysis (MSA)

In the second approach, the MSA, the analysis does not need to perform up to IM amplitudes where all GMs cause collapse. Structured analyses, rather than incremental dynamic analysis, are sometimes performed at a discrete set of IM levels, each with a different GM. Because the GM target parameters change at each IM level, this MSA approach is common when employing the conditional spectrum or another method to choose GM indicative of a specific location considered for the Surat City area (Baker, 2015).

$$P_{\mathrm{M}} = \binom{n_j}{z_j} P_j^{z_j} \left(1 - P_j\right)^{n_j - z_j}, \tag{10}$$

where $\mathrm{P_j}$ is likely to produce fragmentation of the structure with a GM with IM. We aim to find the fragility function that will forecast $\mathrm{P_M}$, and the maximum likelihood finds the fragility function with the best chance of observing the collapse data from structural analysis. When analytical data are collected at several IM levels, the binomial probability product at each IM level provides the opportunity for the whole data set:

$$\mathrm{L(likelihood)} = \prod_{j=1}^{m} P_{\mathrm{M}}. \tag{11}$$

Estimates are derived from the fragility parameters by maximising this probability function. Maximising the logarithm of the probability function is similar and mathematically easier. Therefore, we have:

$$\{\hat{\theta}, \hat{\beta}\} = \underset{\theta,\beta}{\arg\max} \sum_{j=1}^{m} \ln L. \tag{12}$$

Figure 10 shows the derived fragility curve fitting using MSA techniques. The alternative to estimating the fragility function from multiple strip analytical data is to minimise the SSE (sum of squared errors) between actual fractions of collapse and the probability of failure predicted by the fragility function. It is mathematically represented as

$$\{\hat{\theta}, \hat{\beta}\} = \underset{\theta,\beta}{\arg\max} \sum_{j=1}^{m} \left[\frac{z_j}{n_j} - P_j \right]^2. \tag{13}$$

Truncated IDA

Except for the other two methods, the truncated IDA approach did not consider all the selected GM scaled values.

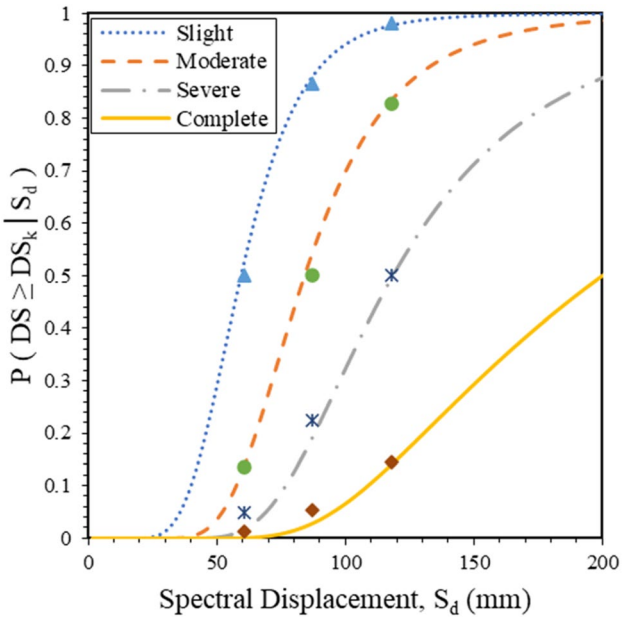

Fig. 9 Fragility curves generated using the NSPA approach

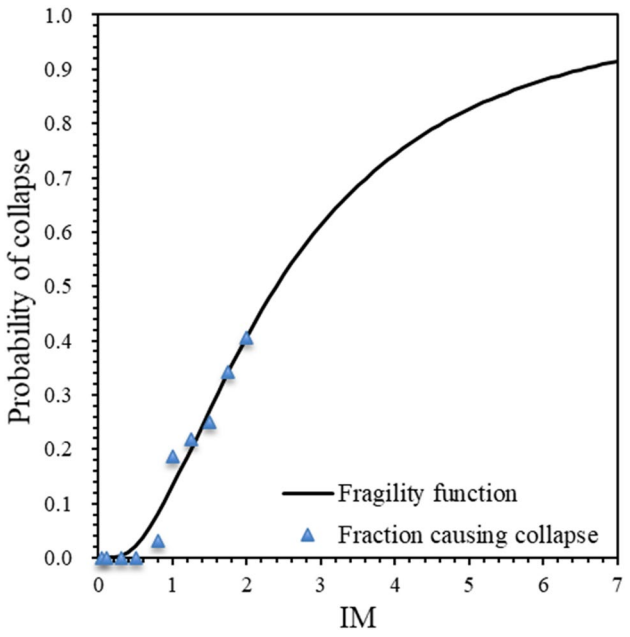

Fig. 10 Observed fractions of collapse as a function of IM and a fragility function estimated using MSA

Instead, it is run an analytical process until the 50% collapse of the RC frame building model. For the m numbers of GMs that were observed to cause failure, their IM values at failure (IM_i) are known. The likelihood that an arbitrary GM causes collapse at IM_i, given a fragility function defined using Eq. (1), is the normal distribution probability density function (PDF). The total n number of GM is subtracted from the m number of collapse GM from that estimate IM_{max}. The likelihood that a given GM can be scaled to IM_{max} without causing failure is the probability that IM_i is greater than IM_{max}:

$$\text{Likelihood} = 1-P. \tag{14}$$

Making the reasonable assumption that the IM_i value for each GM is independent, the likelihood of the entire data set being observed is the product of the individual probabilities:

$$\text{Likelihood} = \prod_{j=1}^{m} P(1-P)^{n-m}. \tag{15}$$

The fragility function parameters are later calculated using this equation by adjusting the parameters until the likelihood function is maximised, as shown in Fig. 11.

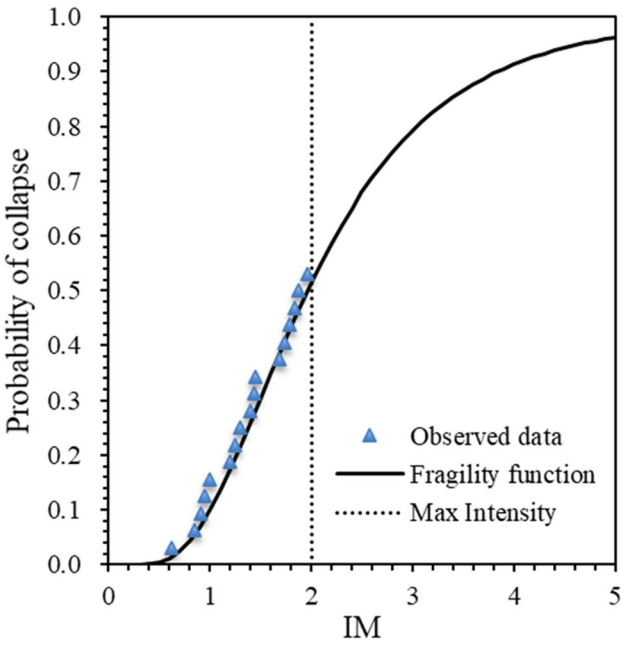

Fig. 11 Observed fractions of collapse as a function of IM and a fragility function estimated using the truncated method

Traditional IDA

The fragility function is fitted to the log-standard normal distribution function with various statistical technical approaches. Serval methods have been established throughout the last two centuries due to advancements in statistical mathematics, efficient hardware support, and higher computation power available to researchers (Baker, 2015; Kiani & Khanmohammadi, 2015; Pitilakis et al., 2014). Linear regression (LR) is traditionally the most used approach to derive the fragility curves. The structural capacity is determined through dynamic time history analyses with increased scaled values, causing the structural behaviour to shift nonlinearly, and finally, the structure will collapse at some point. The RC frame deformation capability against collapse is defined as the final point. As shown in Fig. 12, this procedure generates a set of IM values associated with the commencement of failure for each GM. The fraction of records for which collapse happens at a level lower than x can then be used to estimate the probability of failure at a specific IM level, x. The mean and standard deviation are calculated for the fragility function parameters from this data by taking logarithms of each ground motion's IM value linked with the commencement of collapse:

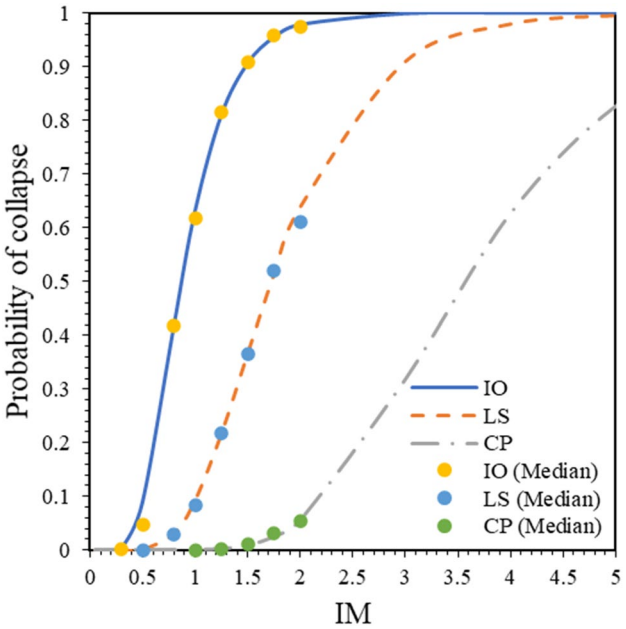

Fig. 12 Observed fractions of collapse as a function of IM and a fragility function estimated using Traditional IDA

$$\ln\hat{\theta} = \frac{1}{n}\sum_{i=1}^{n}\ln IM_i, \tag{16}$$

$$\hat{\beta} = \sqrt{\frac{1}{n-1}\sum_{i=1}^{n}\left(\ln\left(\frac{IM_i}{\hat{\theta}}\right)\right)^2}. \tag{17}$$

In the case of a lognormally distributed variable, the mean of ln IM equals the median of IM. Therefore, utilising the sample mean yield an estimate of θ, Fig. 13 shows a fragility function fitted using this method.

Results and discussion

The current study investigates the efficiency of statistical techniques for constructing seismic fragility curves. Existing circumstances are quite helpful for developing a computationally less expensive and more straightforward process. In accordance with the most recent Indian seismic regulations, a four-storey RC frame structure is chosen for this study. IDA is the most precise and effective method for determining a structure's fragility curve. However, it lacks processing time and requires much upkeep after gathering essential data. Numerous researchers attempt to improve analytic techniques (Baker, 2007, 2015; Cremen & Baker, 2021). The main results of the applications using the various approach to the selected frame can be summarised as follows:

- Intel i5 2.4 GHz computational processor was used in the present study; the overall NSPA for the building studied in the research, including computation of the capacity curve and performance point, is completed in about 500 s. It is considered that generating a complete damage curve necessitates estimating the performance point for the entire duration of an average single damage curve of the same structure, around 120 s. Furthermore, dynamic analysis must be performed for each of the scaled recordings (ten scaled values used), resulting in a total computation time of almost 2400 s, roughly six times the computational cost of the NSPA-based method. It is worth noting that when the number of seismic intensities in the incremental dynamic analysis grows, the gap between the numerical costs also gets bigger.
- The present study minimises the aleatory uncertainty by normalising and scaling the GM. Intensity is not compromised during this process, but the elimination of record-to-record variation prediction of post-earthquake behaviour can be confident.
- A four-storey RC frame building was designed, as per the latest IS 1893:2016 (Part-1), showing the uncertainty value between 0.41 and 0.78 during the IDA and 0.35–0.61 for the NSPA type of analytical approach.
- The MSA and traditional IDA methods are investigated for the same scales of earthquake motions. Although the overall uncertainty variation is considerably high during the MSA approach (see Fig. 14 and Table 8), the truncated approach gives results nearer to the conservative side than the MSA method.

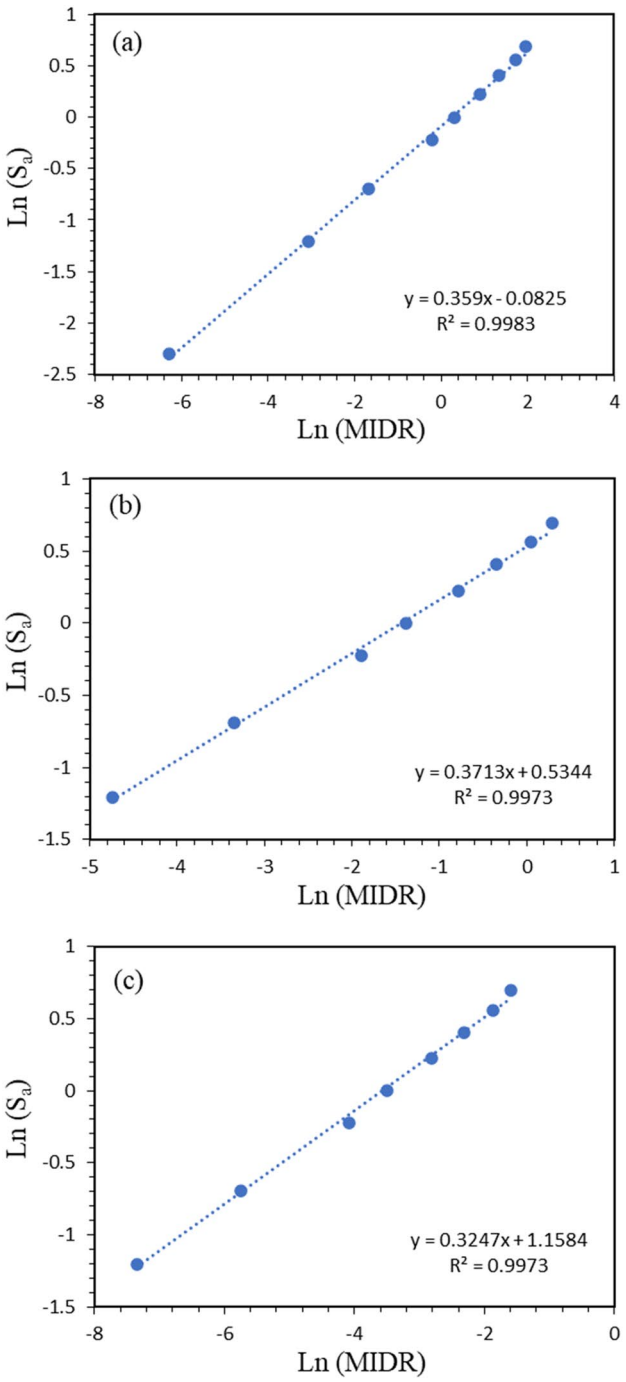

Fig. 13 The linear fitted fragility function between Sa and MIDR for Engineering demand parameter (EDP): **a** 1%, **b** 2%, and **c** 4%

These methods are compared with the coefficient of variation (COV) values and a standard parameter used to compare statistical curve-fitting approaches. Table 8 summarises the fragility parameters obtained with selected seismic fragility curve-fitting methods. CSM is undoubtedly proven to be computationally affordable and easier to perform, but it is only effective if the seismic hazard is

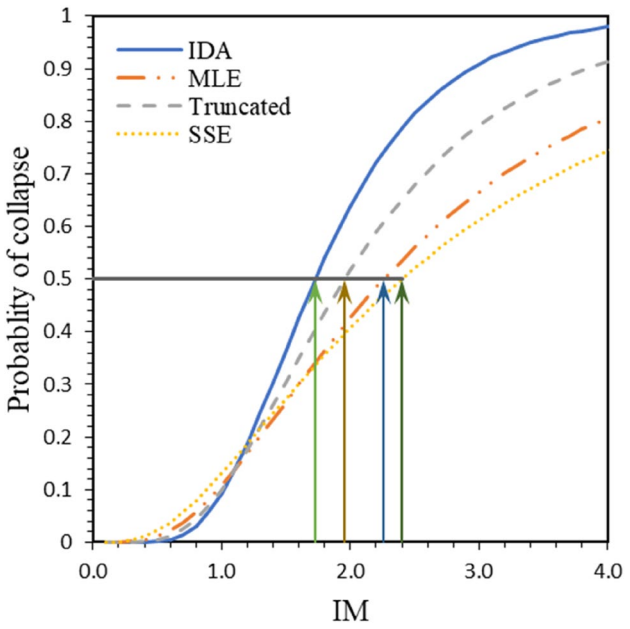

Fig. 14 Comparison of generated fragility curves fitting through various statistical methods

Table 8 The parameters of the fragility curve were found using the traditional IDA, MSA, and truncated methods

Statistical parameters	Traditional IDA	MSA		Truncated IDA
		MLE	SSE	
Mean (μ)	1.73	2.26	2.40	1.96
SD (β)	0.41	0.66	0.78	0.53
COV	0.24	0.29	0.32	0.27

SD standard deviation, *COV* coefficient of variation

precisely characterised. Since the present study's seismic demand is specified using the target response spectrum, NSPA techniques for the resulting fragility curve indicated a 9–12% COV, a considerable uncertainty reduction. The CSM is incapable of addressing seismic demand, and the structural capacity type of the uncertainty estimation, as compared to traditional IDA estimation, is more reasonable.

The traditional IDA approach for deriving the fragility curves shows only 24% variation, while MSA and truncated IDA approach show 29 and 27% of the disparity, respectively. The MSA method is implemented, followed by two other statistical curve-fitting methods, i.e., MLE and SSE. However, the SSE method is ineffective in minimising the error between normal and binomial distribution. MSA and truncated IDA-based approaches necessitated a more time-intensive nonlinear analysis to produce robust results. However, traditional IDA can estimate precisely even with a small sample size.

Conclusions

The impact of fragility curve-fitting methods for structural engineering applications has been highlighted in the current study. MLE, linear regression and SSE have been adopted on the four-storey RC frame buildings among the several appropriate approaches. NSPA and IDA are widely accepted for their accuracy and effectiveness in solving complex structure performance. One of the main goals of this study was to assess the usefulness of the curve-fitting techniques available for deriving fragility curves. In the IDA, uncertainty resulting from RTR variation has also been considered and eliminated by normalising and scaling selected GMs.

It is observed that the expected seismic damage curve highly depends on the analytical approach to determining post-earthquake damage response. The curve-fitting techniques are adapted to fit the fragility curve from the obtained IDA results for the MLE statistical approach, and the final COV is not under engineering tolerance. The traditional IDA method provides around 29% more accurate estimates than other statistical techniques. However, MSA optimised with MLE achieves 9.84% more accurate estimations than the SSE optimisation technique. The obtained results from IDA required a significant amount of computation time, but the outcome was more precise and realistic than NSPA. However, it is also worth noting that a simplified strategy, such as the NSPA, can significantly decrease expensive computational costs. The CSM makes it simple to derive fragility curves compatible with the NSPA and ATC-40 approaches.

All the methods have their pros and cons regarding the type of distribution of data and computational time requirements. NSPA allows a faster and more precise technical approach to examining nonlinear structural behaviour. At the same time, IDA is more expensive in mathematical computational processes and data management. Linear regression and MLE statistical curve-fitting approach provide less uncertainty than the other methods. The current study does not address epistemic uncertainty, which can be decreased by adopting the Monte Carlo and Latin hypercube simulation techniques.

Acknowledgements The authors acknowledge the financial assistance from the Ministry of Human Resource Development (MHRD), the Government of India.

Funding Funding was provided by Ministry of Human Resource Development.

Data availability statement The data supporting this study's findings are available from the corresponding author, Kaushik Gondaliya, upon reasonable request.

Declarations

Conflict of interest On behalf of all authors, the corresponding author states that there is no conflict of interest.

References

Adom-Asamoah, M., & Osei, J. B. (2018). A comparative seismic fragility analysis of a multi and single component beam-column joint models. *Cogent Engineering*. https://doi.org/10.1080/23311916.2018.1426204

American Society of Civil Engineers. (2017). Seismic evaluation and retrofit of existing buildings. American Society of Civil Engineers

Arabzadeh, H., & Galal, K. (2017). Seismic collapse risk assessment and FRP retrofitting of RC coupled C-Shaped core walls using the FEMA P695 methodology. *Journal of Structural Engineering (united States), 143*(9), 1–20. https://doi.org/10.1061/(ASCE)ST.1943-541X.0001820

ATC-40. (1996). Seismic evaluation and retrofit of concrete buildings, report ATC-40 (also Report No. SSC 96-01. California Seismic Safety Commission); Applied Technology Council. Redwood City, CA, USA

Baker, J. W. (2007). Measuring bias in structural response caused by ground motion scaling. *Pacific Conference on Earthquake Engineering, 056*, 1–6. https://doi.org/10.1002/eqe

Baker, J. W. (2015). Efficient analytical fragility function fitting using dynamic structural analysis. *Earthquake Spectra, 31*(1), 579–599. https://doi.org/10.1193/021113EQS025M

Banerjee, A. K., Pramanik, D., & Roy, R. (2016). Seismic structural fragilities: Proposals for improved methodology per spectral matching of accelerogram. *Engineering Structures, 111*, 538–551. https://doi.org/10.1016/j.engstruct.2016.01.002

Barbat, A. H., Pujades, L. G., & Lantada, N. (2008). Seismic damage evaluation in urban areas using the capacity spectrum method: Application to Barcelona. *Soil Dynamics and Earthquake Engineering, 28*(10–11), 851–865. https://doi.org/10.1016/j.soildyn.2007.10.006

Bhandari, M., Bharti, S. D., Shrimali, M. K., & Datta, T. K. (2019). Seismic fragility analysis of base-isolated building frames excited by near- and far-field earthquakes. *Journal of Performance of Constructed Facilities, 33*(3), 1–16. https://doi.org/10.1061/(ASCE)CF.1943-5509.0001298

Bilgin, H. (2016). Generation of fragility curves for typical RC health care facilities: Emphasis on hospitals in Turkey. *Journal of Performance of Constructed Facilities, 30*(3), 1–16. https://doi.org/10.1061/(ASCE)CF.1943-5509.0000806

BIS 875 Part 1. (1987). Design loads (other than earthquake) for buildings and structures. dead loads—code of practice. Bureau of Indian Standards, New Delhi, India

BIS 875 Part 2. (1987). Design loads (other than earthquake) for buildings and structures. Imposed loads—code of practice. Bureau of Indian Standards, New Delhi, India

BIS IS 13920. (2016). Ductile detailing of reinforced concrete-code of practice. Bureau of Indian Standards. New Delhi, India

BIS IS 1893. (2016). Criteria for earthquake resistant design of structures, Part-1 general provisions and buildings. Bureau of Indian Standards. New Delhi, India

BIS IS 456. (2000). Indian standard code of practice for plain and reinforced concrete, Bureau of Indian Standards. New Delhi, India

Choudhury, T., & Kaushik, H. B. (2018). Seismic fragility of open ground storey RC frames with wall openings for vulnerability assessment. *Engineering Structures, 155*(June 2017), 345–357. https://doi.org/10.1016/j.engstruct.2017.11.023

Cremen, G., & Baker, J. W. (2021). Variance-based sensitivity analyses and uncertainty quantification for FEMA P-58 consequence predictions. *Earthquake Engineering & Structural Dynamics, 50*(3), 811–830. https://doi.org/10.1002/eqe.3370

Dabaghi, M., Saad, G., & Allhassania, N. (2019). Seismic collapse fragility analysis of reinforced concrete shear wall buildings. *Earthquake Spectra, 55*(1), 383–404. https://doi.org/10.1193/121717EQS259M

FEMA/NIBS methodology (HAZUS®-MH MR5). (2003). Advanced engineering building module: technical and user's manual, Federal Emergency Management Agency, Washington DC, USA

Jeon, J. S., DesRoches, R., Brilakis, I., & Lowes, L. N. (2012). Aftershock fragility curves for damaged non-ductile reinforced concrete buildings. *Proceedings of the 15th World Conference on Earthquake Engineering*, August 2015, Paper No. 0909. https://doi.org/10.13140/2.1.5055.6484

Ji, J., Elnashai, A. S., & Kuchma, D. A. (2007). An analytical framework for seismic fragility analysis of RC high-rise buildings. *Engineering Structures, 29*(12), 3197–3209. https://doi.org/10.1016/j.engstruct.2007.08.026

Kappos, A. J., Panagopoulos, G., Panagiotopoulos, C., & Penelis, G. (2006). A hybrid method for the vulnerability assessment of R/C and URM buildings. *Bulletin of Earthquake Engineering, 4*(4), 391–413. https://doi.org/10.1007/s10518-006-9023-0

Kiani, J., & Khanmohammadi, M. (2015). New approach for selection of real input ground motion records for incremental dynamic analysis (IDA). *Journal of Earthquake Engineering, 19*(4), 592–623. https://doi.org/10.1080/13632469.2014.997901

Kiani, J., & Pezeshk, S. (2017). Sensitivity analysis of the seismic demands of RC moment resisting frames to different aspects of ground motions. *Earthquake Engineering and Structural Dynamics, 46*(15), 2739–2755. https://doi.org/10.1002/eqe.2928

Kyriakides, N. C., & Pantazopoulou, S. J. (2018). Collapse fragility curves for RC buildings exhibiting brittle failure modes. *Journal of Structural Engineering (United States), 144*(2), 1–11. https://doi.org/10.1061/(ASCE)ST.1943-541X.0001920

Lantada, N., Pujades, L. G., & Barbat, A. H. (2009). Vulnerability index and capacity spectrum based methods for urban seismic risk evaluation. A comparison. *Natural Hazards*, *51*(3), 501–524. https://doi.org/10.1007/s11069-007-9212-4

Luco, N., & Cornell, C. A. (2007). Structure-specific scalar intensity measures for near-source and ordinary earthquake ground motions. *Earthquake Spectra, 23*(2), 357–392. https://doi.org/10.1193/1.2723158

Mander, J. B., Priestley, M. J. N., & Park, R. (1988). Theoretical stress-strain model for confined concrete. *Journal of Structural Engineering, 114*(8), 1804–1826. https://doi.org/10.1061/(ASCE)0733-9445(1988)114:8(1804)

McCrum, D. P., Amato, G., & Suhail, R. (2016). Development of seismic fragility functions for a moment resisting reinforced concrete framed structure. *The Open Construction and Building Technology Journal, 10*(1), 42–51. https://doi.org/10.2174/1874836801610010042

Menegotto, M., & P. E. Pinto. (1973). Method of analysis for cyclically loaded RC plane frames including changes in geometry and non-elastic behaviour of elements under combined normal force and bending. Symposium on the resistance and ultimate deformability of structures acted on by well defined repeated loads. *International Association for Bridge and Structural Engineering. Zurich, Switzerland*. pp. 15–22.

Mitropoulou, C. C., Kostopanagiotis, C., Kopanos, M., Ioakim, D., & Lagaros, N. D. (2016). Influence of soil-structure interaction on fragility assessment of building structures. *Structures, 6*, 85–98. https://doi.org/10.1016/j.istruc.2016.02.005

Mohanty, W. K., & Verma, A. K. (2013). Probabilistic seismic hazard analysis for Kakrapar atomic power station, Gujarat, India. *Natural Hazards, 69*(1), 919–952. https://doi.org/10.1007/s11069-013-0744-5

Moon, D.-S., Lee, Y.-J., & Lee, S. (2018). Fragility analysis of space reinforced concrete frame structures with structural irregularity in Plan. *Journal of Structural Engineering, 144*(8), 04018096. https://doi.org/10.1061/(asce)st.1943-541x.0002092

Nazari, Y. R., & Saatcioglu, M. (2017). Seismic vulnerability assessment of concrete shear wall buildings through fragility analysis. *Journal of Building Engineering, 12*(June), 202–209. https://doi.org/10.1016/j.jobe.2017.06.006

Pejovic, J., & Jankovic, S. (2016). Seismic fragility assessment for reinforced concrete high-rise buildings in Southern Euro-Mediterranean zone. *Bulletin of Earthquake Engineering, 14*(1), 185–212. https://doi.org/10.1007/s10518-015-9812-4

Pitilakis, K. D., Karapetrou, S. T., & Fotopoulou, S. D. (2014). Consideration of aging and SSI effects on seismic vulnerability assessment of RC buildings. *Bulletin of Earthquake Engineering, 12*(4), 1755–1776. https://doi.org/10.1007/s10518-013-9575-8

Porter, K. (2014). Encyclopedia of earthquake engineering. *Encyclopedia of Earthquake Engineering*. https://doi.org/10.1007/978-3-642-36197-5

Prota, A., Cicco, F., & Cosenza, E. (2009). Cyclic behavior of smooth steel reinforcing bars: Experimental analysis and modeling issues. *Journal of Earthquake Engineering, 13*(4), 500–519.

Sairam, B., Singh, A. P., Patel, V., Chopra, S., & Kumar, M. R. (2019). VS30 mapping and site characterisation in the seismically active intraplate region of Western India: Implications for risk mitigation. *Near Surface Geophysics, 17*(5), 533–546. https://doi.org/10.1002/nsg.12066

Saruddin, S. N. A., & Nazri, F. M. (2015). Fragility curves for low- and mid-rise buildings in Malaysia. *Procedia Engineering, 125*, 873–878. https://doi.org/10.1016/j.proeng.2015.11.056

Serdar Kirçil, M., & Polat, Z. (2006). Fragility analysis of mid-rise R/C frame buildings. *Engineering Structures, 28*(9), 1335–1345. https://doi.org/10.1016/j.engstruct.2006.01.004

Sharma, V., Shrimali, M. K., Bharti, S. D., & Datta, T. K. (2021a). Seismic energy loss in semi-rigid steel frames under near-field earthquakes. In: S. K. Saha, M. Mukherjee (Eds.), *Recent advances in computational mechanics and simulations* (Vol. 103, pp. 431–443). Springer, Singapore. https://doi.org/10.1007/978-981-15-8138-0_33

Sharma, V., Shrimali, M. K., Bharti, S. D., & Datta, T. K. (2021b). Seismic fragility evaluation of semi-rigid frames subjected to near-field earthquakes. *Journal of Constructional Steel Research*. https://doi.org/10.1016/j.jcsr.2020.106384

Shukla, J., & Choudhury, D. (2012). Estimation of seismic ground motions using deterministic approach for major cities of Gujarat. *Natural Hazards and Earth System Science, 12*(6), 2019–2037. https://doi.org/10.5194/nhess-12-2019-2012

Su, L., Li, X. L., Jiang, Y., & Pang, Y. (2020). Comparison of methodologies for seismic fragility analysis of unreinforced masonry buildings considering epistemic uncertainty. *Engineering Structures, 205*(2019), 110059. https://doi.org/10.1016/j.engstruct.2019.110059

Surana, M., Singh, Y., & Lang, D. H. (2015). Seismic performance of shear-wall and shear-wall core buildings designed for Indian codes. *Advances in Structural Engineering: Dynamics, Volume Two, 43*, 1229–1241. https://doi.org/10.1007/978-81-322-2193-7_96

Surana, M., Singh, Y., & Lang, D. H. (2018). Seismic characterisation and vulnerability of building stock in hilly regions. *Natural Hazards Review, 19*(1), 1–16. https://doi.org/10.1061/(ASCE)NH.1527-6996.0000275

Tavazo, H. A., & Ranjbaran, A. (2017). Fragility analysis of 3D reinforced concrete frames based on endurance time method with derived standard deviation. *Journal of Earthquake and Tsunami, 11*(4), 1–23. https://doi.org/10.1142/S1793431117500117

Thaker, T. P., Rathod, G. W., Rao, K. S., & Gupta, K. K. (2012). Use of seismotectonic information for the seismic hazard analysis for Surat city, Gujarat, India: Deterministic and probabilistic approach. *Pure and Applied Geophysics, 169*(1–2), 37–54. https://doi.org/10.1007/s00024-011-0317-z

Vamvatsikos, D., & Allin Cornell, C. (2002). Incremental dynamic analysis. *Earthquake Engineering and Structural Dynamics, 31*(3), 491–514. https://doi.org/10.1002/eqe.141

Verki, A. M., & Aval, S. B. B. (2020). Performance-based design through implementation of FEMA P-58 methodology in developing countries. *Open Journal of Earthquake Research, 09*(03), 255–272. https://doi.org/10.4236/ojer.2020.93015

ZakerEsteghamati, M., Banazadeh, M., & Huang, Q. (2018). The effect of design drift limit on the seismic performance of RC dual high-rise buildings. *Structural Design of Tall and Special Buildings, 27*(8), 1–16. https://doi.org/10.1002/tal.1464